

Chapter 4

Rigid Body Equilibrium Grasps

Any grasping system ought to fulfill three requirements. First, the fingers must hold the object at an equilibrium grasp. Second, the grasp should be stable with respect to arbitrary small position and force perturbations. Third, the grasp should withstand finite disturbance sets serving as a model for the intended application. This chapter focuses on the equilibrium grasp requirement. The chapter begins with a description of the common rigid-body contact models. Each contact model is associated with a particular collection of forces that can be transmitted at a rigid-body contact. The chapter next focuses on the multi-contact setting where k finger bodies $\mathcal{O}_1 \dots \mathcal{O}_k$ hold an object \mathcal{B} at an equilibrium grasp. The chapter introduces the *grasp map*, which gives the net wrenches that can be applied to \mathcal{B} by varying the finger forces at the contacts. The chapter then formulates the equilibrium grasp condition: a k -contact arrangement forms a *feasible equilibrium grasp* if some finger force combination satisfying the contact model constraints can affect a zero net wrench on the grasped object. The chapter subsequently discusses the notion of *internal squeeze forces* associated with an equilibrium grasp. Finally, a *moment labeling* technique for depicting the net wrenches that can be affected by planar grasps is described. This representation will prove useful in subsequent chapters.

4.1 Rigid Body Contact Models

In general, a *contact model* describes the possible forces that can be transmitted between a finger body and the grasped object when the two are in contact. A *rigid body contact model* describes the possible physical interaction when the two bodies are assumed to be perfectly rigid. This section introduces the most commonly used rigid body contact models. While no real objects are truly rigid, rigid body models provide an excellent idealization in many grasping and fixturing applications. However, high load applications such as workpiece machining as well as fingertips made of compliant material require a consideration of contact deformations. Part IV of this book focuses on compliant contact models and their use in grasp and fixture analysis.

We shall focus on the physical interaction between two perfectly rigid bodies, the object \mathcal{B} and a finger body \mathcal{O}_i , under the assumption that the two bodies are in point contact.

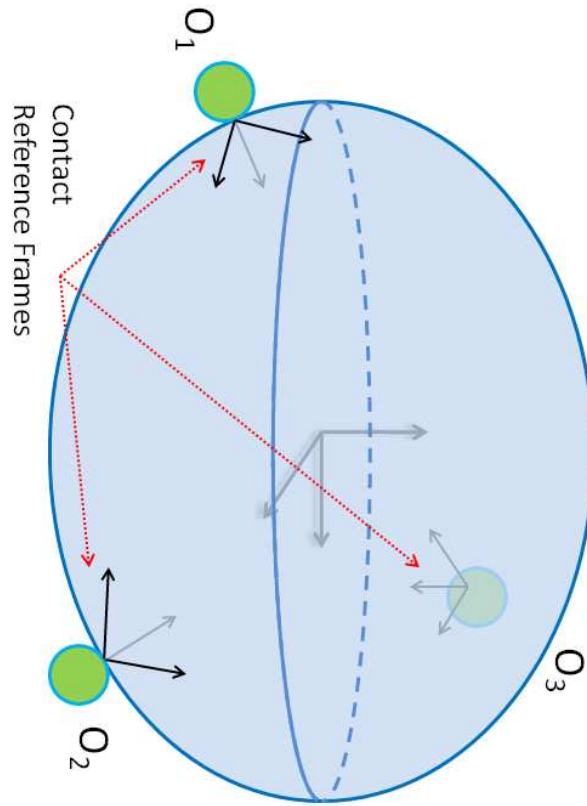


Figure 4.1: Depiction of contact reference frames and body-fixed reference frame.

In the following description of the contact models, we assume that \mathcal{B} lies at its nominal configuration q_0 , with the contact point located at x_i , as expressed in the world frame coordinates. We also assume that \mathcal{B} 's frame origin coincides with the world frame origin at q_0 . Under this assumption the torque generated by a force f_i acting on \mathcal{B} at x_i is simply $x_i \times f_i$ (see Lemma ?? and the exercises below). We will describe the inter-body forces using a local reference frame based at the i^{th} contact. One axis of this frame is the inward pointing unit normal to \mathcal{B} at x_i , denoted n_i . The remaining two axes are unit tangents to \mathcal{B} at x_i , denoted s_i and t_i , such that $\{s_i, t_i, n_i\}$ forms a right-handed frame (see Figure 4.1). The following are the most common rigid body contact models.

1. The Frictionless Point Contact Model

The simplest rigid body contact model assumes that the contact is entirely frictionless. While no practical contact between two bodies is truly frictionless, this model serves as a conservative approximation in cases of low contact friction and variable surface traction. Additionally, as we shall see in Part II, many problems in the analysis of frictionless grasps can be answered with purely geometric methods. Therefore the study of frictionless grasps serves as a convenient starting point for a more general study of grasping mechanics.

At a frictionless contact, the inter-body force can only be sustained along the direction normal to the contacting bodies' surfaces. The contact force is thus given by $f_i = f_i^n n_i$, where f_i^n is a non-negative scalar. Note that f_i^n is non-negative because a finger tip can only apply *a unilateral pushing force* at the contact. The collection of forces supported by a frictionless point contact, denoted C_i , is thus given by

$$C_i = \{f_i \in \mathbb{R}^m : f_i = f_i^n n_i \text{ for } f_i^n \geq 0\},$$

where $m = 2$ in 2D and $m = 3$ in 3D. Note that C_i forms a half-line, or a one-dimensional cone, based at x_i and pointing along \mathcal{B} 's inward normal n_i .

2. The Point Contact with Coulomb Friction Model

Any real bodies in contact experience friction, which is a force resisting the relative motion of the contacting bodies. The field of *tribology* studies the science and technologies related to interacting surfaces in motion. Complex tribological models that predict the frictional forces between two bodies may include electrostatic effects, weak chemical bonding effects, and mechanical interaction of microscopic asperities. These models, while accurate, are too cumbersome for practical grasp and fixture analysis.

Charles-Augustin Coulomb introduced a simple empirical friction model which was derived from experiments like the one depicted in Figure 4.2(a). Consider a block of mass m made from material A (say aluminum) resting under the influence of gravity on a flat surface made from material B (say steel). We assume that the materials have been cleaned of any surface residue and dirt, and that both materials are dry. Starting at time $t=0$, the block is pulled with a force f_p parallel to the horizontal surface. Imagine that the pulling force is linearly increased from zero. Since the block is under the influence of gravity, a frictional reaction force, f_r , will arise from the interaction of the two contacting surfaces. Figure 4.2(b) shows a typical graph of f_r versus f_p that results from such experiments.

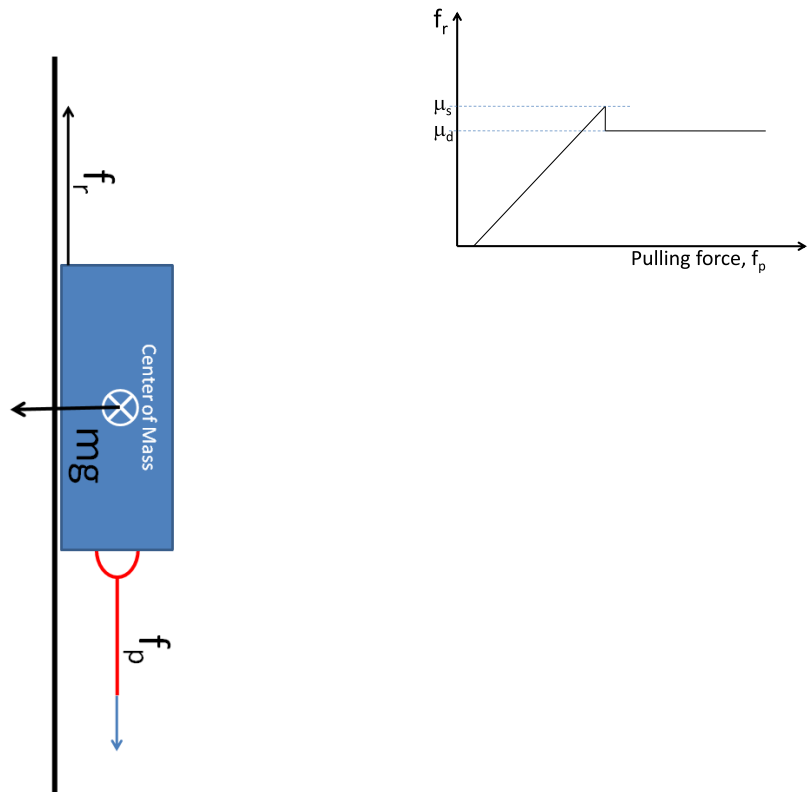


Figure 4.2: (a) A schematic diagram of Coulomb's friction experiment. (b) A typical plot of the normalized reaction force f_r versus the pulling force f_p , showing both static and dynamic friction effects.

Initially the block remains at rest, even under the influence of an increasing pulling force. This implies that the frictional reaction force f_r exactly counterbalances the pulling force f_p during the initial ramp up of the applied force. However, as the increasing pulling force reaches a magnitude f_p^* (whose value depends upon the block's mass and the choice of materials A and B), the block begins to slide in the direction of f_p . Experiments with different block masses (but the same materials), show that the ratio f_p^*/mg is roughly a constant, which is termed the Coulomb static friction coefficient, μ_s . Once the block begins to slide, the magnitude of f_r drops slightly, but remains constant even when f_p is further increased. The reaction force magnitude is modeled in this case by the product of a constant dynamic Coulomb friction coefficient, μ_d , times mg . In most materials the difference between μ_s and μ_d is small, and to a reasonable approximation a single *Coulomb friction coefficient* value, $\mu = \mu_s$, is used to model both effects. Moreover, our analysis of frictional rigid body grasps will focus on the limits of frictional force that can be obtained when the finger tips do not slide upon the object's surface. Therefore, $\mu = \mu_s$ will form the basis of the frictional contact models used throughout this book.

The friction coefficient is a non-negative parameter whose value varies across material types and increases with surface roughness. The friction coefficient of metal-on-metal contacts typically varies in the range of $0.1 \leq \mu \leq 0.5$. For teflon-on-teflon contacts the friction coefficient can be as low as $\mu = 0.04$. A contact between rubber and common materials such as plastic, metal, or wood achieves high friction coefficient values in the range of $1.0 \leq \mu \leq 2.0$.

Exercise. Figure 4.3 shows a simple procedure to estimate the Coulomb friction coefficient. Place a block of mass m on the inclined slope which is inclined at an angle α with respect to the direction of gravity. As the angle of the slope is slowly increased, the block begins to slide at a critical angle, α^* . Show that the critical angle can be related to the Coulomb friction coefficient, μ , as follows:

$$\alpha^* = \tan^{-1}(\mu) . \quad (4.1)$$

Solution. Gravity induces a force normal to the contact surface whose magnitude is $f_n = mg \cos \alpha$. Similarly, gravity also ‘‘pulls’’ or ‘‘pushes’’ the block down the slope with a force of magnitude $f_p = mg \sin \alpha$. If the block is stationary when the slope angle is α , then the frictional reaction force, f_r , is equal to f_p , and the contact obeys the no-slip condition of the Coulomb friction law: $|f_p| \leq \mu f_n$. As the slope angle is slowly increased, the block will begin to slide at a critical angle, α^* . At this critical angle, $f_r = \mu f_n$. This implies that $mg \sin \alpha^* = \mu mg \cos \alpha^*$, which gives (4.1). We shall see in Chapter 5 that this *friction angle*, α^* , plays an important role in grasp and fixture analysis.

Returning to the contact model, let (f_i^s, f_i^t, f_i^n) be the tangential and normal components of the force f_i with respect to the i^{th} contact frame, $(f_i^s, f_i^t) = (f_i \cdot s_i, f_i \cdot t_i)$ and $f_i^n = f_i \cdot n_i$. Under the static Coulomb friction law, the finger tip can still apply only a unilateral pushing force along the contact normal direction, so that $f_i^n \geq 0$ as before. The presence of friction additionally allows the finger to independently apply tangential force components. However, if the magnitude of the tangential force becomes too large, the finger tip will begin to slide on the object surface. The Coulomb friction model states that the finger tip will not slip

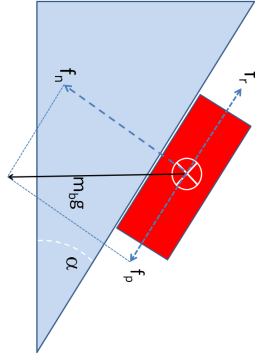


Figure 4.3: An alternative procedure to empirically determine the Coulomb friction coefficient.

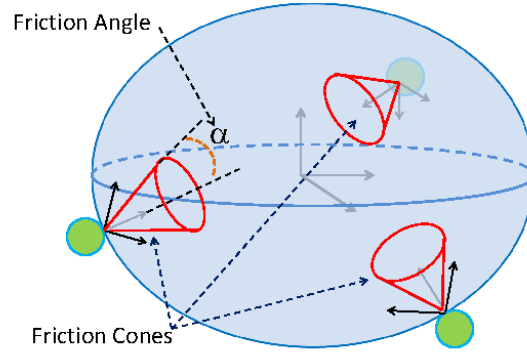


Figure 4.4: The friction cone associated with the frictional point contact model.

on \mathcal{B} 's surface as long as $\|f_i^s s_i + f_i^t t_i\| \leq \mu f_i^n$, where μ is the friction coefficient. Once the finger force violates this condition, the finger tip will start to slide on \mathcal{B} 's surface, with the magnitude of the tangent reaction force satisfying the equality $\|f_i^s s_i + f_i^t t_i\| = \mu f_i^n$, such that the direction of the tangent reaction force opposes the finger's sliding direction.

Based on this discussion, the collection of forces supported by a *frictional point contact*, denoted C_i , is given in the 3D case by

$$C_i = \left\{ f_i \in \mathbb{R}^3 : f_i \cdot n_i \geq 0, \sqrt{(f_i \cdot s_i)^2 + (f_i \cdot t_i)^2} \leq \mu f_i \cdot n_i \right\},$$

where $\{s_i, t_i, n_i\}$ is the local frame at the i^{th} contact and μ is the friction coefficient. The corresponding collection of forces is given in the 2D case by

$$C_i = \left\{ f_i \in \mathbb{R}^2 : f_i \cdot n_i \geq 0, |f_i \cdot t_i| \leq \mu f_i \cdot n_i \right\},$$

where $\{t_i, n_i\}$ is the local frame at the i^{th} contact and μ is the friction coefficient. See Figure 4.6 for an example of a planar grasp making use of frictional point contacts.

Figure 4.5: Idealized geometry of a contact patch associated with a soft point contact model.

Friction Cone Interpretation. In general, a set C forms a *cone* if for any $v_1, v_2 \in C$ the positive linear combination $\lambda_1 v_1 + \lambda_2 v_2$ lies in C for all $\lambda_1, \lambda_2 \geq 0$. The collection of forces C_i has a nice geometric interpretation in terms of a *friction cone* (Figure 4.4). Consider the cone whose apex is located at the contact point x_i , and whose central axis is aligned with \mathcal{B} 's inward pointing normal n_i . Let $\alpha = \tan^{-1}(\mu)$ be the half-angle of this cone. As long as the force applied by the finger lies inside this friction cone, the finger tip will not slip at the contact. When the finger tip applies a force outside the friction cone, it will slide tangentially along the surface of \mathcal{B} . The finger force in this case consists of a force component which acts on \mathcal{B} along the friction cone edge, and a complementary tangential force which affects the finger's own dynamics during sliding.

3. The Soft Point Contact Model

While this chapter focuses on rigid body contact models, let us consider what happens when a finger tip which is made from a compliant material comes into contact with a solid object. The finger material will deform in the vicinity of the contact, resulting in a contact “patch” rather than a unique point of contact (see Figure 4.5). In the 3D case, the contact will be established along a two-dimensional region which can sustain some torsional forces of interaction about the contact normal. The soft point contact model approximately accounts for these torsional forces within the rigid body modeling framework. The potential effect of finger tip softness, adapted to the rigid body point contact framework, adds to the frictional point contact model an independently modulated torque, τ_i^n , which acts about the contact normal. This torque is physically generated when a finger tip rotation about the contact normal is opposed by the integrative effect of Coulomb friction acting at each point in the contact patch area. To a rough approximation, the norm of this torque is bounded according to: $|\tau_i^n| \leq \gamma f_i^n$, where $\gamma > 0$ is called the *rotational friction coefficient*. The collection of forces and torques supported by a *soft point contact* model is thus given by

$$C_i = \left\{ (f_i, \tau_i^n) \in \mathbb{R}^3 \times \mathbb{R} : f_i \cdot n_i \geq 0, \sqrt{(f_i \cdot s_i)^2 + (f_i \cdot t_i)^2} \leq \mu f_i \cdot n_i, |\tau_i^n| \leq \gamma \right\},$$

where $\{s_i, t_i, n_i\}$ is the local frame at the i^{th} contact, and μ and γ are the two friction coefficients. Note that C_i forms a *generalized* friction cone in the space of force and torque components. A two-finger grasp making use of soft point contacts is depicted in Figure 4.7.

The rotational friction coefficient. While the Coulomb friction coefficient is a unitless parameter, the relation $|\tau_i^n| \leq \gamma f_i^n$ indicates that γ has units of length. A rough approximation for γ can be obtained as follows. Let us assume that the contact area is a planar disc of radius R , centered at the i^{th} contact and tangent to \mathcal{B} at the contact. Let us further assume that the normal inter-body force component, f_i^n , is evenly distributed over the

contact area (it is actually maximal at x_i and decays to zero on the disc's boundary). The normal force at each point of the contact area is thus $f_n = f_i^n / (\pi R^2)$. Let the finger tip now attempt to rotate about the contact normal, n_i , such that all points of the contact area are on the verge of slipping. Assuming that Coloumb friction acts at the individual points of the contact area, the torque generated at the individual points about n_i satisfies the equality $|\tau(r)| = \mu r f_n$, where $r \in [0, R]$. When this torque is integrated over the contact area, the net torque generated by the contact is $|\tau_i^n| = \frac{2}{3} \mu R f_i^n$. It follows that $\gamma = \frac{2}{3} \mu R$, where R is the contact area radius and μ is the Coloumb friction coefficient. We see that γ is proportional to R which has length units.

4.2 The Grasp Map

Our objective in this section is to develop an expression for the net wrench affected on \mathcal{B} by the k fingers $\mathcal{O}_1 \dots \mathcal{O}_k$. Let \mathbf{w}_i be the wrench generated by the i^{th} finger, described in the fixed world reference frame. It consists of a wrench generated by the finger force, f_i , together with a possible torque τ_i^n about \mathcal{B} 's contact normal n_i ,

$$\mathbf{w}_i = \begin{pmatrix} f_i \\ x_i \times f_i \end{pmatrix} + \begin{pmatrix} \vec{0} \\ \tau_i^n \end{pmatrix} = \begin{bmatrix} I \\ [x_i \times] \end{bmatrix} f_i + \begin{pmatrix} \vec{0} \\ n_i \end{pmatrix} \tau_i^n.$$

Note that in the 2D case $[x_i \times] = x_i^T J$ is a row vector. The net grasping wrench affecting \mathcal{B} is simply the sum of the wrenches generated by the individual fingers:

$$\mathbf{w} = \sum_{i=1}^k \mathbf{w}_i = \begin{bmatrix} I & \cdots & I \\ [x_1 \times] & \cdots & [x_k \times] \end{bmatrix} \begin{pmatrix} f_1 \\ \vdots \\ f_k \end{pmatrix} + \begin{bmatrix} \vec{0} & \cdots & \vec{0} \\ n_1 & \cdots & n_k \end{bmatrix} \begin{pmatrix} \tau_1^n \\ \vdots \\ \tau_k^n \end{pmatrix}, \quad (4.2)$$

where the second summand appears only under the soft point contact model.

Each of the finger forces and torques in (4.2) has an associated set of constraints: C_i describes the forces and torques that can be supported at the i^{th} contact. The *composite* generalized friction cone for the grasp, defined by $C_1 \times \dots \times C_k$,¹ describes the set of all feasible forces and torques at the contacts. It follows that (4.2) defines a mapping, called the *grasp map*, which maps the forces-and-torques in $C_1 \times \dots \times C_k$ to the net grasping wrench affecting \mathcal{B} . The net wrench affecting \mathcal{B} varies in the cotangent space $\mathbf{w} \in T_{q_0}^* \mathbb{R}^m$ ($m=3$ or 6), which we shall call *wrench space*. A formal definition of the grasp map follows.

Definition 1 (Grasp Map). *Let rigid finger bodies $\mathcal{O}_1 \dots \mathcal{O}_k$ contact a rigid object \mathcal{B} . Let C_i be the cone of feasible forces and torques at the i^{th} finger contact. The rigid body **grasp map** is the linear map $G : C_1 \times \dots \times C_k \rightarrow T_{q_0}^* \mathbb{R}^m$ specified by (4.2),*

$$\mathbf{w} = \begin{bmatrix} I & \cdots & I \\ [x_1 \times] & \cdots & [x_k \times] \end{bmatrix} \begin{pmatrix} f_1 \\ \vdots \\ f_k \end{pmatrix} + \begin{bmatrix} \vec{0} & \cdots & \vec{0} \\ n_1 & \cdots & n_k \end{bmatrix} \begin{pmatrix} \tau_1^n \\ \vdots \\ \tau_k^n \end{pmatrix}, \quad (4.3)$$

¹Given subsets $\mathcal{S}_1, \dots, \mathcal{S}_k$ of \mathbb{R}^n , the product $\mathcal{S}_1 \times \dots \times \mathcal{S}_k$ is the subset of $\mathbb{R}^n \times \dots \times \mathbb{R}^n$ defined by $\mathcal{S}_1 \times \dots \times \mathcal{S}_k = \{(s_1, \dots, s_k) : s_i \in \mathcal{S}_i \text{ for } i=1 \dots k\}$.

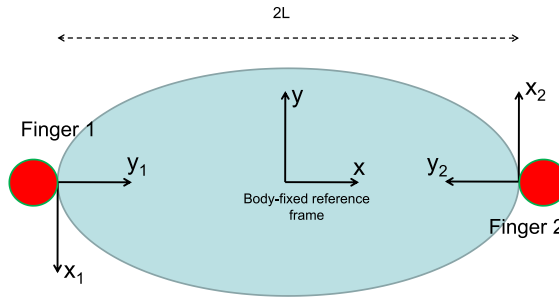


Figure 4.6: A planar two-finger frictional grasp of an ellipse.

where the first summand appears in all three contact models while the second summand appears only in the soft point contact model.

Recall that a linear map can be represented as a matrix in terms of bases for its domain and image spaces. Let us obtain such a matrix representation for the grasp map G in terms of force and torque components for the composite friction cone. Let p be the number of independent force and torque components at each of the k contacts. Let $\bar{f}_i \in \mathbb{R}^p$ denote the corresponding vector of force and torque components, and let $\bar{f} = (\bar{f}_1, \dots, \bar{f}_k) \in \mathbb{R}^{kp}$ be the composite vector of force and torque components. The $m \times kp$ matrix representing G , denoted \bar{G} , maps the composite vector \bar{f} to the net wrench affecting \mathcal{B} , $\mathbf{w} = \bar{G}\bar{f}$. Under the frictionless point contact model, $\bar{f}_i = f_i^n$ for $i = 1 \dots k$, and \bar{G} is the $m \times k$ matrix:

$$\bar{G} = \begin{bmatrix} n_1 & \dots & n_k \\ x_1 \times n_1 & \dots & x_k \times n_k \end{bmatrix}.$$

Note that \bar{G} is fully determined by the contact locations, $x_1 \dots x_k$, and by the contact normals $n_1 \dots n_k$. Under the frictional point contact model, say in the 3D case, $\bar{f}_i = (f_i^s, f_i^t, f_i^n)$ for $i = 1 \dots k$, and \bar{G} is the $m \times 3k$ matrix:

$$\bar{G} = [\bar{G}_1 \ \dots \ \bar{G}_k] \quad \text{where} \quad \bar{G}_i = \begin{bmatrix} s_i & t_i & n_i \\ x_i \times s_i & x_i \times t_i & x_i \times n_i \end{bmatrix} \quad \text{for } i = 1 \dots k.$$

The grasp matrix associated with frictional contacts depends on $x_1 \dots x_k$ as well as the contact frames, $\{s_i, t_i, n_i\}$ for $i = 1 \dots k$. Last, under the soft point contact model $\bar{f}_i = (f_i^s, f_i^t, f_i^n, \tau_i^n)$ for $i = 1 \dots k$, and \bar{G} is the $m \times 4k$ matrix:

$$\bar{G} = [\bar{G}_1 \ \dots \ \bar{G}_k] \quad \text{where} \quad \bar{G}_i = \begin{bmatrix} s_i & t_i & n_i & \vec{0} \\ x_i \times s_i & x_i \times t_i & x_i \times n_i & n_i \end{bmatrix} \quad \text{for } i = 1 \dots k.$$

Example: Figure 4.6 shows a planar two-finger grasp of an elliptical object along its major axis, whose length is $2L$. Assuming frictional point contacts, each finger can independently modulate two force components. The grasp matrix is determined by the contact positions $x_1 = (-L, 0)$ and $x_2 = (L, 0)$, and by the contact frames $\{t_1, n_1\} = \left\{ \begin{pmatrix} 0 \\ -1 \end{pmatrix}, \begin{pmatrix} 1 \\ 0 \end{pmatrix} \right\}$ and $\{t_2, n_2\} = \left\{ \begin{pmatrix} 0 \\ 1 \end{pmatrix}, \begin{pmatrix} -1 \\ 0 \end{pmatrix} \right\}$. The net grasping wrench affecting the ellipse results from application of the

Figure 4.7: A two-finger grasp of a rectangular box where each contact is governed by the soft finger model.

3×4 grasp matrix \bar{G} on the four independent finger force components:

$$\mathbf{w} = [\bar{G}_1 \quad \bar{G}_2] \begin{pmatrix} \bar{f}_1 \\ \bar{f}_2 \end{pmatrix} = \begin{bmatrix} 0 & 1 & 0 & -1 \\ -1 & 0 & 1 & 0 \\ L & 0 & L & 0 \end{bmatrix} \begin{pmatrix} f_1^t \\ f_1^n \\ f_2^t \\ f_2^n \end{pmatrix}.$$

Note that $\bar{G} = [\bar{G}_1 \quad \bar{G}_2]$ has full rank for this grasp. It follows that the fingers can in principle generate any desired net wrench on \mathcal{B} . Equivalently, G maps the composite cone $C_1 \times C_2$ onto \mathcal{B} 's wrench space. This is an example of a *force closure* grasp, a topic which is explored in Chapter Z.

Example: Figure 4.7 shows a 3D grasp involving two fingers grasping a rectangular box at the center of opposite faces, where the box size is $2L$. The two contacts are governed by the soft point contact model. Each of the two fingers can independently control *four* contact force components: normal force, two tangential force components, and torque about the contact normal. The grasp matrix \bar{G} is 6×8 , and the net grasping wrench on \mathcal{B} is:

$$\mathbf{w} = [\bar{G}_1 \quad \bar{G}_2] \begin{pmatrix} \bar{f}_1 \\ \bar{f}_2 \end{pmatrix} = \begin{bmatrix} 1 & 0 & 0 & 0 & 1 & 0 & 0 & 0 \\ 0 & 0 & 1 & 0 & 0 & 0 & -1 & 0 \\ 0 & -1 & 0 & 0 & 0 & 1 & 0 & 0 \\ 0 & L & 0 & 0 & 0 & L & 0 & 0 \\ 0 & 0 & 0 & 1 & 0 & 0 & 0 & -1 \\ L & 0 & 0 & 0 & -L & 0 & 0 & 0 \end{bmatrix} \begin{pmatrix} f_1^s \\ f_1^t \\ f_1^n \\ \tau_1^n \\ f_2^s \\ f_2^t \\ f_2^n \\ \tau_1^n \end{pmatrix}$$

Here, too, the matrix $\bar{G} = [\bar{G}_1 \quad \bar{G}_2]$ has full rank, implying that the two fingers can generate any desired net wrench on \mathcal{B} . This is another example of a *force closure* grasp (see Chapter Z).

Exercise 5.7: Consider a planar two-finger equilibrium grasp having frictional contacts. Can the 3×4 grasp matrix G of this grasp ever lose its full rank of three?

Solution: The grasp matrix represents the grasp map which is given by

$$\mathbf{w} = \mathbf{w}_1 + \mathbf{w}_2 = \begin{bmatrix} I & I \\ x_1^T J & x_2^T J \end{bmatrix} \begin{pmatrix} f_1 \\ f_2 \end{pmatrix} \quad f_i \in C_i \text{ for } i = 1, 2$$

, where I is a 2×2 identity matrix and $J = \begin{bmatrix} 0 & -1 \\ 1 & 0 \end{bmatrix}$. Any linear combination of the upper two rows has the form $(v, v) \in \mathbb{R}^4$. The lower row can have the form (v, v) only when $x_1 = x_2$, which is physically unrealizable. Therefore, the grasp matrix of any planar two-finger equilibrium grasp with frictional contacts always have a full rank of three.

4.3 The Equilibrium Grasp Condition

Let us now characterize the situation where the fingers hold the object \mathcal{B} at an equilibrium grasp. We shall restrict our attention to the simplest scenario where \mathcal{B} is influenced solely by the fingers, without any external influences such as gravity. The maintenance of an equilibrium grasp under gravity will be discussed in subsequent chapters. A k -contact arrangement forms a *feasible equilibrium grasp* if the fingers can apply non-vanishing forces and torques consistent with the contact model, such that the net wrench affecting \mathcal{B} is zero.

Definition 2 (Equilibrium Grasp). *Let a rigid object \mathcal{B} be contacted by rigid finger bodies $\mathcal{O}_1 \dots \mathcal{O}_k$ at the points $x_1 \dots x_k$. The contact arrangement forms a **feasible equilibrium grasp** under the frictionless/frictional point contact models if there exist non-zero forces $f_1 \dots f_k$ satisfying the condition:*

$$G \begin{pmatrix} f_1 \\ \vdots \\ f_k \end{pmatrix} = \begin{pmatrix} f_1 \\ x_1 \times f_1 \end{pmatrix} + \dots + \begin{pmatrix} f_k \\ x_k \times f_k \end{pmatrix} = \vec{0} \quad f_i \in C_i \text{ for } i=1 \dots k, \quad (4.4)$$

where G is the grasp map and C_i is the cone of feasible forces at x_i for $i = 1 \dots k$.

The contact arrangement forms a **feasible equilibrium grasp** under the soft point contact model if there exist non-vanishing forces $f_1 \dots f_k$ and torques $\tau_1^n \dots \tau_k^n$ satisfying the condition:

$$G \begin{pmatrix} f_1 \\ \tau_1^n \\ \vdots \\ f_k \\ \tau_k^n \end{pmatrix} = \begin{pmatrix} f_1 \\ x_1 \times f_1 + \tau_1^n n_1 \end{pmatrix} + \dots + \begin{pmatrix} f_k \\ x_k \times f_k + \tau_k^n n_k \end{pmatrix} = \vec{0} \quad (f_i, \tau_i^n) \in C_i \text{ for } i=1 \dots k,$$

where G is the grasp map and C_i is the generalized friction cone at x_i for $i = 1 \dots k$.

Note that in the 2D case $x_i \times f_i = x_i^T J f_i$ is a scalar. Since an equilibrium grasp involves a balancing action of opposing forces and torques, all equilibrium grasps involve at least *two* contacts. A feasible equilibrium grasp requires that G will map some non-vanishing combination of forces and torques to the zero wrench. This observation highlights an important property of equilibrium grasps: in order to maintain an equilibrium, the contacts should be selected such that G has a non-zero kernel. The forces and torques in the kernel of G are called *internal grasp forces*, with the understanding that they possibly include internal grasp torques about the contact normals. The internal grasp forces are discussed in the next section.

Let us now interpret the equilibrium condition (4.4), associated with the “hard” point contact models, directly in \mathcal{B} ’s wrench space. Let the i^{th} *wrench cone*, \mathcal{W}_i , be the collection of wrenches generated by the i^{th} contact as its force varies in C_i , $\mathcal{W}_i = \{(f_i, x_i \times f_i) : f_i \in C_i\}$. Each \mathcal{W}_i forms a cone based at the wrench space origin. For instance, at a planar frictional point contact C_i is bounded by two edges, and the corresponding wrench cone forms a two-dimensional sector bounded by the wrenches generated by the friction cone edges; see Figure 4.8. The collection of net wrenches that can be affected on \mathcal{B} is the sum $\mathcal{W}_1 + \dots + \mathcal{W}_k$. This set still forms a cone in wrench space (see exercise). However, at a feasible equilibrium

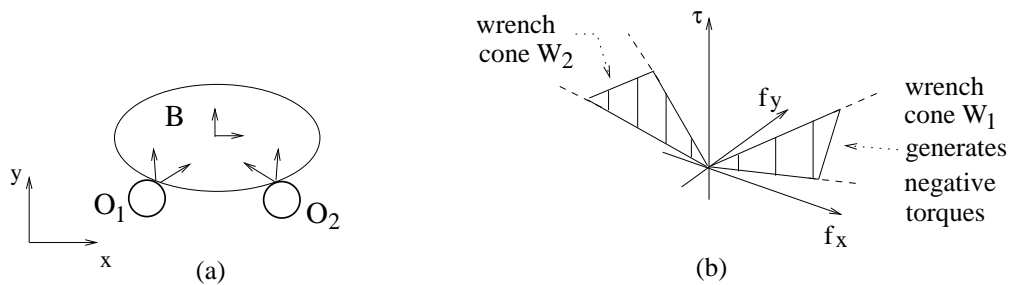


Figure 4.8: A frictional 2-contact arrangement which is not a feasible equilibrium grasp.

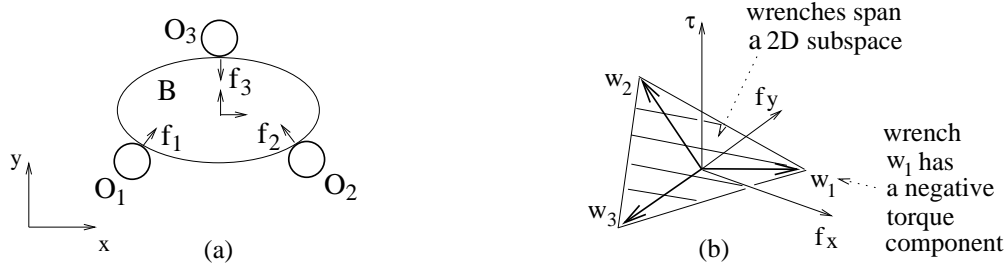


Figure 4.9: A frictionless 3-contact arrangement which is a feasible equilibrium grasp.

grasp $\mathcal{W}_1 + \dots + \mathcal{W}_k$ contains a non-trivial *subspace* passing through the wrench space origin. The following examples illustrate this property.

Example: Consider the two-contact arrangement depicted in Figure 4.8(a). Assuming *frictional* point contacts, the sum $\mathcal{W} = \mathcal{W}_1 + \mathcal{W}_2$ is a semi-infinite tetrahedral cone pointing away from the origin; see Figure 4.8(b). It follows that this contact arrangement is not a feasible equilibrium grasp.

Example: Next consider the three-contact arrangement depicted in Figure 4.9(a). Assuming *frictionless* point contacts, each wrench cone is a semi-infinite ray aligned with the c-obstacle normal $\eta_i(q_0)$ ($i = 1, 2, 3$). In this case the set $\mathcal{W}_1 + \mathcal{W}_2 + \mathcal{W}_3$ forms a two-dimensional subspace passing through the wrench space origin; see Figure 4.9(b). This contact arrangement is a feasible equilibrium grasp.

Essential Contacts: A contact is said to be *essential* for the grasp if it must generate a non-vanishing force in order to maintain the equilibrium. When all k contacts are essential, the sum $\mathcal{W}_1 + \dots + \mathcal{W}_k$ becomes a $(k-1)$ -dimensional subspace passing through the wrench space origin. For instance, the three contacts in the grasp of Figure 4.9 are all essential, and the set $\mathcal{W}_1 + \mathcal{W}_2 + \mathcal{W}_3$ spans a two-dimensional subspace. A graphical technique for depicting the wrench cones associated with planar grasps, called *moment labeling*, is described at the end of this chapter.

4.4 The Internal Grasp Forces

We have seen that the grasp map possesses a non-trivial kernel at an equilibrium grasp.² If the kernel of G is non-empty, the forces and torques in the kernel are called *internal grasp forces*, as these forces and torques are absorbed by the grasped object without disturbing the equilibrium grasp. *We shall see in the next chapter that these internal forces play an important role in high quality grasps.*

Let us determine the dimension of the kernel of G under the various contact models and discuss some examples which provide an intuitive feel for these forces. Let us first determine the *generic* dimension of the kernel of G . Recall that \bar{G} is the $m \times kp$ matrix representing G , where $m = 3$ or 6 , $k \geq 2$ is the number of contacts, and $p \geq 1$ is the number of force components at each of the k contacts. When \bar{G} has full rank, its rank is given by $\text{rank}(\bar{G}) = \min\{m, kp\}$. Assuming that p and m are constant for a given grasping application, there are two cases to consider according to the value of k . In the first case the number of contacts is small such that $kp \leq m$. In this case $\text{rank}(\bar{G}) = kp$. Since the grasp map generates non-vanishing equilibrium forces, it must have a non-empty kernel at the equilibrium grasp. Consider now the contact arrangements obtained by locally perturbing the contacts of the equilibrium grasp along the surface of \mathcal{B} . Except for very rare situations, \bar{G} would assume full rank at the perturbed contact arrangements, such that its rank drops precisely by *one* at the nominal equilibrium grasp. It follows that $\dim(\ker(\bar{G})) = 1$ in the case where $kp \leq m$. Next consider the case where the number of contacts is large such that $kp > m$. In this case $\text{rank}(\bar{G}) = m$, and consequently $\dim(\ker(\bar{G})) = kp - m > 1$.

Let us first characterize the internal forces under the *frictionless* point contact model. Each contact can only modulate its normal force component, and \bar{G} is $m \times k$. As long as $k \leq m + 1$ i.e., $2 \leq k \leq 4$ in 2D and $2 \leq k \leq 7$ in 3D, the internal grasp forces span only a one-dimensional subspace. This subspace consists of a coordinated modulation of the grasp's *total preload*, defined as the totality of the force magnitudes, $f_T = \sum_{i=1}^k f_i^n$ (see exercise). The dimension of the internal force subspace increases for higher numbers of contacts. However, we shall see in subsequent chapters that $k \leq m + 1$ contacts provide perfectly adequate grasps for almost all rigid objects, even under slippery contact conditions.

Next consider the *frictional* point contact model. Under this model \bar{G} is $3 \times 2k$ in 2D and $6 \times 3k$ in 3D. Based on the generic formula, the internal forces span one-dimensional subspace only in the case of $k = 2$ contacts, both in 2D and 3D. Much like the frictionless case, these forces can only modulate of the total preload f_T . For higher number of contacts, $\dim(\ker(\bar{G})) = 2k - 3$ in 2D and $\dim(\ker(\bar{G})) = 3k - 6$ in 3D. It is interesting to observe that in the 2D case $2k - 3$ is precisely the number of bars required for interconnecting k point masses such that the resulting structure forms a single connected rigid body (see exercises). The internal forces associated with three frictional contacts are illustrated with the following example.

Example: Consider a planar equilibrium grasp of an object \mathcal{B} by three frictional contacts. The grasp matrix \bar{G} is 3×6 in this case, implying that \bar{G} has a three-dimensional kernel of

²Recall that the *kernel* of a linear map G is the linear subspace satisfying $Gv = \vec{0}$. The image of G is also a linear subspace, and the *rank* of G is the dimension of this subspace.

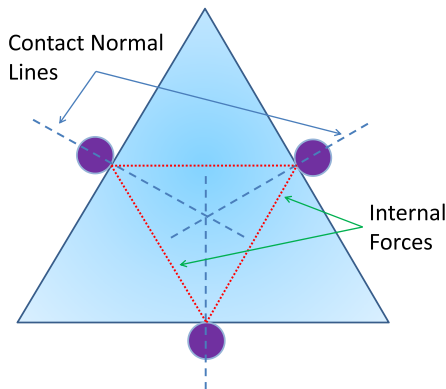


Figure 4.10: Grasp of a planar equilateral triangular object using three frictional point contacts.

internal grasp forces. The forces (f_1, f_2, f_3) spanning the kernel are given by

$$\ker(\bar{G}) = \text{span} \left\{ \begin{pmatrix} x_2 - x_1 \\ -(x_2 - x_1) \\ \vec{0} \end{pmatrix}, \begin{pmatrix} \vec{0} \\ x_3 - x_2 \\ -(x_3 - x_2) \end{pmatrix}, \begin{pmatrix} x_1 - x_3 \\ \vec{0} \\ -(x_1 - x_3) \end{pmatrix} \right\}.$$

In contrast with the two-contact grasps, the internal grasp forces do not merely modulate the equilibrium force magnitudes, but actually rotate the equilibrium force directions within the permissible friction cones (see exercise 3.x).

Exercise: Consider a planar equilibrium grasp consisting of three frictional point contacts on the midpoints of each face of an equilateral triangle (Figure 4.10).

- (a) Construct the grasp, G , and show that it is full rank. Consequently, the null space of G is a three-dimensional vector space.
- (b) Show that the null space can be spanned by three basis vectors, where each internal force basis vector physically corresponds to a pair of opposing forces of equal magnitude applied along the line connecting the pair of contact points. Note that this result generalizes to three point planar frictional grasps which do not necessarily have the equilateral triangular geometry.
- (c) Note that the internal force vectors in **Part (a)** may not lie inside the friction cones of the contact, and therefore may not be feasible contact forces. Show that a null space vector consisting of only normal forces at each contact (all with the same magnitude) is feasible.

Solution. (a) Assign a reference frame whose origin is located at the point where the three contact normal lines intersect, and whose orientation is parallel to that of the contact frame of finger #1. In this reference frame, the grasp map takes the form:

$$\begin{aligned}
G &= \begin{pmatrix} \vec{n}_1 & \vec{t}_1 & \vec{n}_2 & \vec{t}_2 & \vec{n}_3 & \vec{t}_3 \\ -D(\vec{n}_1 \times \vec{n}_1) & -D(\vec{n}_1 \times \vec{t}_1) & -D(\vec{n}_2 \times \vec{n}_2) & -D(\vec{n}_2 \times \vec{t}_2) & -D(\vec{n}_3 \times \vec{n}_3) & -D(\vec{n}_3 \times \vec{t}_3) \end{pmatrix} \\
&= \begin{pmatrix} 0 & 1 & \frac{\sqrt{3}}{2} & -\frac{1}{2} & -\frac{\sqrt{3}}{2} & -\frac{1}{2} \\ 1 & 0 & -\frac{1}{2} & -\frac{\sqrt{3}}{2} & -\frac{1}{2} & -\frac{\sqrt{3}}{2} \\ 0 & D & 0 & D & 0 & D \end{pmatrix} \tag{4.5}
\end{aligned}$$

where $D = L/(2\sqrt{3})$, and the set of contact forces are: $\vec{f} = (f_1^n \ f_1^t \ f_2^n \ f_2^t \ f_3^n \ f_3^t)^T$. Note that the first, second, and fourth column of this matrix are linearly independent vectors, and thus the grasp map has full rank.

(b) Consider the application of equal forces, having magnitude F , along the line connecting finger contacts points 1 and 2. The finger contact force in this case is:

$$\vec{f} = F \begin{pmatrix} \frac{\sqrt{3}}{2} & -\frac{1}{2} & \frac{\sqrt{3}}{2} & \frac{1}{2} & 0 & 0 \end{pmatrix}^T. \tag{4.6}$$

Direct multiplication of matrix (4.5) times the finger contact force vector (4.6) yields a zero net wrench on the triangular object, confirming that this is an internal force vector. By symmetry, the forces of equal magnitude along the lines connecting the other two possible pairs of contact points can also be shown to be squeeze forces.

(c) A force of magnitude F applied along each of the three contact normals, $\vec{f} = F (1 \ 0 \ 1 \ 0 \ 1 \ 0)^T$ is a feasible contact force in the null space of the grasp map G in Equation (4.5).

Finally, under the *soft* point contact model the internal forces also include torques about the contact normal. In this case \vec{G} is $6 \times 4k$. Since $k \geq 2$, the kernel of \vec{G} is a $(4k - 6)$ -dimensional subspace. Note that the internal forces and torques span at least a two-dimensional subspace, as illustrated in the following example.

Example. Let us revisit the example where two soft point contacts grasp a rectangular box, depicted in Figure 4.7. The grasp matrix \vec{G} is 6×8 in this example, and its kernel is a two-dimensional subspace. One basis vector of the kernel is given by $(f_1^s, f_1^t, f_1^n, \tau_1^n, f_2^s, f_2^t, f_2^n, \tau_1^n) = (0, 0, 1, 0, 0, 0, 1, 0)$. It corresponds to opposing finger forces squeezing \mathcal{B} along the line connecting the two contact points. The other basis vector of the kernel is given by $(f_1^s, f_1^t, f_1^n, \tau_1^n, f_2^s, f_2^t, f_2^n, \tau_1^n) = (0, 0, 0, 1, 0, 0, 0, 1)$. This particular basis vector is possible only under the soft point contact model, as it consists of opposing finger torques squeezing \mathcal{B} about the line connecting the two contact points.

Let us end this section with a physical interpretation of the internal grasp forces associated with k frictional contacts.

Physical interpretation of the internal grasp forces: First consider the planar grasps. The grasp matrix associated with k frictional point contacts is a $3 \times 2k$ matrix. This matrix has generically full rank, and its kernel is a $(2k - 3)$ -dimensional subspace of *internal grasp forces*, $(f_1, \dots, f_k) \in \ker G$. The dimension of the kernel of G , $2k - 3$, happens to be the minimum number of rigid bars required to connect k point masses into a rigid planar structure

Figure 4.11: (a) A rigid structure connecting $k = 8$ points with $3k - 6 = 18$ bars. (b) Its transformation to a rigid structure connecting $k = 7$ points with $3k - 6 = 15$ bars.

(see exercises 3.19-3.20 for a formal proof). This observation can be intuitively explained as follows. Suppose the object \mathcal{B} is a planar graph whose nodes are the k point masses and whose edges are rigid bars connected by revolute joints at the nodes. When the graph forms a rigid structure, the bars can absorb any combination of internal grasp forces acting at the k nodes. In this case any combination of internal grasp forces acting at the k nodes, $(f_1, \dots, f_k) \in \ker G$, can be expressed as a sum of opposite forces acting along the $2k - 3$ bars. The dimension of the kernel of G is therefore at most $2k - 3$. Now suppose the structure is minimal, so that each of the $2k - 3$ bars is necessary for maintaining rigidity. When any single bar is removed, the structure is incapable of absorbing at least one combination of internal grasp forces. The $2k - 3$ bars thus represent a *basis* for the subspace of internal grasp forces of the k -finger grasp.

In the case of spatial grasps, the grasp matrix associated with k frictional point contacts is a $6 \times 3k$ matrix. When the grasp involves $k \geq 3$ fingers, G has generically full rank and a $(3k - 6)$ -dimensional kernel of internal grasp forces, $(f_1, \dots, f_k) \in \ker G$. This dimension is again the minimum number of rigid bars required to connect k spatial point masses into a rigid spatial structure. Let us demonstrate this fact with a construction procedure. Let the object \mathcal{B} be a spatial graph whose nodes are the k point masses, and whose edges are rigid bars connected by spherical joints at the nodes.³ Since each rigid bar is attached to spherical joints at its endpoints, one cannot prevent self-rotation of the bar about its axes. Hence we will construct a spatial graph whose bars freely rotate about their axes, such that the graph as a whole forms a rigid structure. The construction is based on the fact that a triangle with spherical joints forms a rigid structure up to self-rotation of its bars. When k is even, split the k point masses into two sets of $k/2$ points, then embed these sets in two parallel planes. Next connect the points of each subset into a rigid planar graph as discussed above. This task can be achieved with a total of $k - 3$ bars per planar graph. Next arrange the two planar graphs on top of each other and connect the vertically aligned points with $k/2$ vertical bars. Finally, add a diagonal bar within each vertical rectangle using $k/2$ additional bars. The resulting spatial graph is triangulated and has a total of $2(k - 3) + \frac{k}{2} + \frac{k}{2} = 3k - 6$ bars. When k is odd, first construct the spatial graph for $k + 1$ point masses, then contract a pair of adjacent points and their connecting bar to a single point. During the contraction, identify each pair of bars that connect the two original points with a common third point of the structure into a single bar. The resulting spatial graph is still triangulated and has $3k - 6$ bars. As verified in exercises 4.x-4.y, in both cases the structure is rigid up to self-rotation of the bars, and contains the minimum number of bars required for structural rigidity.

Example: The structure connecting $k = 8$ point masses into a rigid body is shown in Figure 4.11(a). Note that this structure consists of $3k - 6 = 18$ bars. Let us next contract the point x_8 toward x_7 along their connecting bar, as depicted in Figure 4.11(a). During this contraction the pairs of bars marked as 'a' and 'b' merge into two single bars. The resulting

³A spherical joint can be imagined as a bar ending with a ball which freely rotates inside a spherical socket. This joint has *three* degree of freedom, since the bar can point in any direction as well as rotate about its axis.

seven-point structure possesses $3k - 6 = 15$ bars as shown in Figure 4.11(b). The resulting structure graphically represents a basis for the subspace of internal grasp forces associated with grasps whose contacts are located at the seven point masses.

4.5 The Moment Labeling Technique

This section describes a *moment labeling* technique which allows us to graphically depict the collection of grasp wrenches affecting \mathcal{B} in planar contact arrangements.⁴ The technique can graphically determine if a contact arrangement is a feasible equilibrium grasp, and if it is a feasible equilibrium, to determine the dimension of the subspace spanned by the net grasp wrenches. The technique is also useful in non-static applications such as part insertion [1].

Recall that the collection of net grasp wrenches is the sum of the finger wrench cones, $\mathcal{W}_1 + \dots + \mathcal{W}_k$. The moment labeling technique is based on a duality between the sum of the cones and the intersection of their polar cones. Let us first describe this duality and then apply it to our problem. Let W be a cone based at the origin of \mathbb{R}^m . That is, W has the property that for any $w_1, w_2 \in W$ the positive linear combination $s_1 w_1 + s_2 w_2$ lies in W for all $s_1, s_2 \geq 0$. It is intuitively clear that the intersection of two cones is still a cone based at the origin. The *sum* of two cones, which is equivalent to their convex hull,⁵ is the set $W_1 + W_2 = \{w_1 + w_2 : w_1 \in W_1, w_2 \in W_2\}$. The sum of two cones is also a cone based at the origin. The cone *polar* to W , denoted W' , consists of all vectors pointing away from W ,

$$W' = \{v \in \mathbb{R}^m : w \cdot v \leq 0 \text{ for all } w \in W\}. \quad (4.7)$$

For instance, when W is a two-dimensional sector based at the origin of \mathbb{R}^3 , its polar cone W' is the three-dimensional wedge depicted in Figure 4.12(a). The following lemma describes a duality property between cone summation and polar cone intersection.

Lemma 4.5.1 (Cone Duality). *Let W_1 and W_2 be two cones based at the origin of \mathbb{R}^m , and let W_1' and W_2' be their polar cones. The sum $W_1 + W_2$ is **polar** to the intersection $W_1' \cap W_2'$.*

Proof: Let v be a vector in the intersection of the polar cones, $v \in W_1' \cap W_2'$. By definition of polarity, $w_1 \cdot v \leq 0$ for all $w_1 \in W_1$ and $w_2 \cdot v \leq 0$ for all $w_2 \in W_2$. Hence v satisfying the inequality: $(w_1 + w_2) \cdot v = w_1 \cdot v + w_2 \cdot v \leq 0$ for all $w_1 \in W_1$ and $w_2 \in W_2$. It follows that $W_1' \cap W_2'$ is polar to the summation cone $W_1 + W_2$. \square

The duality property is illustrated in Figure 4.12(b). The figure shows a tetrahedral cone generated by the sum of two sectors, and its polar cone generated by the intersection of the wedges polar to the individual sectors. Let us now put the cones mentioned in the lemma in the context of our problem. Since \mathcal{B} is assumed to be a planar object, its configuration space is parametrized by $q \in \mathbb{R}^3$. Let q_0 be \mathcal{B} 's configuration, and recall that $T_{q_0} \mathbb{R}^3 \cong \mathbb{R}^3$ is the

⁴The term *moment* means torque about a specific axis. In 2D it is the torque about an axis perpendicular to the plane.

⁵A set \mathcal{S} in \mathbb{R}^m is *convex* if for any $x_1, x_2 \in \mathcal{S}$ the line segment connecting x_1 and x_2 lies in \mathcal{S} . The *convex hull* of two sets is the smallest convex set containing the two sets.

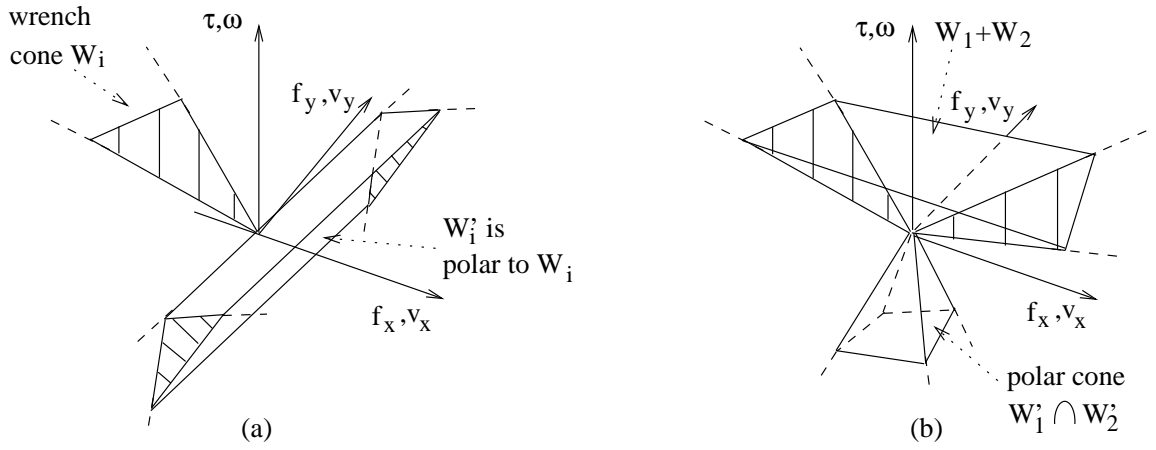


Figure 4.12: (a) A wrench cone \mathcal{W}_i and its polar cone \mathcal{W}_i' . (b) The net wrench cone $\mathcal{W}_1 + \mathcal{W}_2$ and its polar cone $\mathcal{W}_1' \cap \mathcal{W}_2'$.

c-space tangent space at q_0 . In the following discussion W will represent a cone of wrenches embedded in $T_{q_0} \mathbb{R}^3$, while its polar cone, W' , will represent a cone of tangent vectors in $T_{q_0} \mathbb{R}^3$. To emphasize that W is a cone of wrenches while W' is a cone of tangent vectors, we will say that W and W' are *dual* cones. Note that the Euclidean inner product in (4.7) represents the action, or instantaneous work, of a wrench on a tangent vector. The dual cone W' can thus be interpreted as the set of \mathcal{B} 's instantaneous motions impeded by *all* the wrenches of W .

Let \mathcal{W}_i be the i^{th} finger wrench cone, and let \mathcal{W}_i' be its polar cone for $i = 1 \dots k$. Based on the duality property, the sum $\mathcal{W}_1 + \dots + \mathcal{W}_k$ is polar to the intersection $\mathcal{W}_1' \cap \dots \cap \mathcal{W}_k'$. Therefore, our plan is to first obtain a graphical depiction of the polar cones $\mathcal{W}_1', \dots, \mathcal{W}_k'$, take their intersection, then use duality to depict the sum $\mathcal{W}_1 + \dots + \mathcal{W}_k$. The wrench cone \mathcal{W}_i is a two-dimensional sector given by $\mathcal{W}_i = \{(f_i, x_i \times f_i) : f_i \in C_i\}$, where C_i is the physical friction cone at x_i (Figure 4.12(a)). For planar objects, the friction cone C_i can be written as a positive linear combination of its two edges,

$$C_i = \{s_1 f^L + s_2 f^R : s_1, s_2 \geq 0\},$$

where f^L and f^R are unit forces aligned with the two edges of C_i . It follows that \mathcal{W}_i can be written as a positive linear combination of the wrenches generated by f^L and f^R ,

$$\mathcal{W}_i = \left\{ s_1 \begin{pmatrix} f_i^L \\ x_i \times f_i^L \end{pmatrix} + s_2 \begin{pmatrix} f_i^R \\ x_i \times f_i^R \end{pmatrix} : s_1, s_2 \geq 0 \right\}.$$

Equivalently, \mathcal{W}_i is the sum $\mathcal{W}_i = \mathcal{W}_i^L + \mathcal{W}_i^R$, where \mathcal{W}_i^L and \mathcal{W}_i^R are the one-dimensional wrench cones generated by $(f_i^L, x_i \times f_i^L)$ and $(f_i^R, x_i \times f_i^R)$. Using $(\mathcal{W}_i^L)'$ and $(\mathcal{W}_i^R)'$ to denote the polar cones of \mathcal{W}_i^L and \mathcal{W}_i^R , we will obtain \mathcal{W}_i' as the intersection $\mathcal{W}_i' = (\mathcal{W}_i^L)' \cap (\mathcal{W}_i^R)'$.

So consider for a moment the one-dimensional wrench cone generated by a unit force f acting on \mathcal{B} at a point x , given by $W_f = \{s(f, x \times f) : s \geq 0\}$. The polar cone of W_f , given by $W_f' = \left\{ \dot{q} \in T_{q_0} \mathbb{R}^3 : \begin{pmatrix} f \\ x \times f \end{pmatrix} \cdot \dot{q} \leq 0 \right\}$, is a halfspace passing through q_0 , bounded

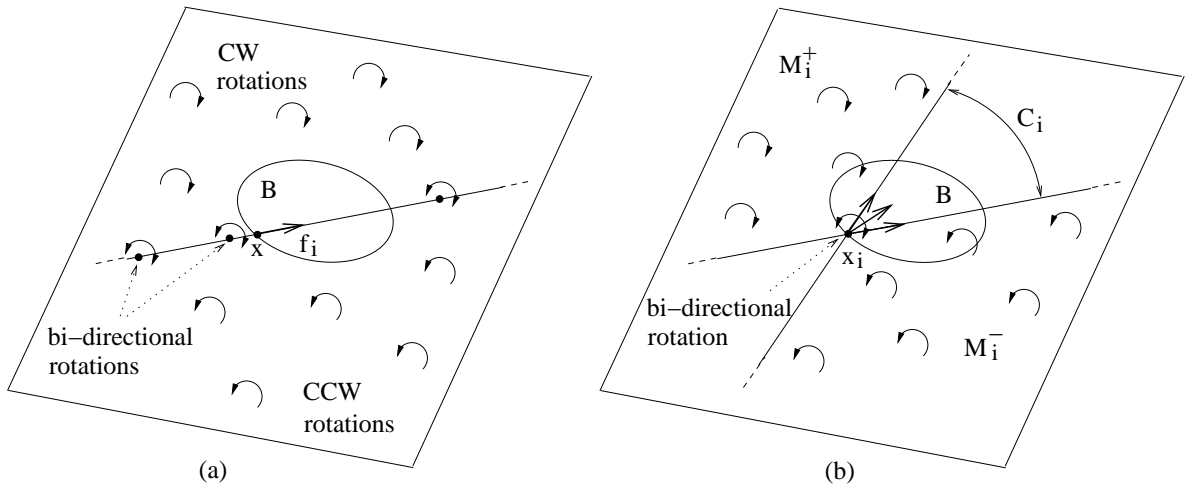


Figure 4.13: (a) The instantaneous rotation halfplanes represent the halfspace polar to the wrench $(f, x \times f)$. (b) The polygons M_i^- and M_i^+ represent the cone W_i^polar polar to the wrench sector W_i .

by the plane orthogonal to $(f, x \times f)$ and pointing away from this wrench. We encountered a similar halfspace in Section ??, in the context of the c-space obstacles. We argued there that the halfspace of $T_{q_0} \mathbb{R}^3$ pointing away from the c-obstacle (i.e. the halfspace containing the c-obstacle outward normal) consists of instantaneous clockwise rotations of B about points on the right side of the contact normal line, counterclockwise rotations on the left side of the contact normal line, and bi-directional rotations on the contact normal line itself. The tangent vectors in the opposite halfspace correspond to opposite instantaneous rotations of B . The same characterization holds for the halfspace pointing away from any fixed wrench $(f, x \times f)$ based at q_0 (see exercise 4.x). As depicted in Figure 4.13(a), this halfspace consists of instantaneous clockwise rotations of B on the left side of the force line, counterclockwise rotations on the right side of the force line, and bi-directional rotations on the force line itself. These instantaneous rotation halfplanes graphically represent the halfspace *polar* to a one-dimensional wrench cone.

Exercise: Let W_f be the one-dimensional cone generated by a wrench $(f, x \times f)$. Prove that the instantaneous rotations representing the halfspace *polar* to W_f are clockwise rotations on the left side of the force line, counterclockwise rotations on the right side of the force line, and bi-directional rotations on the force line itself (Figure 4.13(a)).

Solution: Let y be B 's instantaneous center of rotation associated with a tangent vector \dot{q} . Based on the proof of 4.5.2, the tangent vectors $\dot{q} = (v, \omega) \in T_{q_0} \mathbb{R}^3$ can be parametrized in terms of y and ω by the formula $\dot{q} = \omega(y \times e, e)$, where $(y, \omega) \in \mathbb{R}^2 \times \mathbb{R}$. Substituting for \dot{q} in the polarity condition (4.7) gives

$$\begin{pmatrix} f \\ x \times f \end{pmatrix} \cdot \dot{q} = \omega(f, x \times f) \begin{pmatrix} y \times e \\ e \end{pmatrix} = \omega((x - y) \times f) \cdot e \leq 0.$$

Since e is a unit vector perpendicular to the plane, the polarity condition is equivalent to the planar inequality $\omega(x - y) \times f \leq 0$. There are now two cases to consider. When $\omega \leq 0$ the object B executes a clockwise rotation about y . In this case $(x - y) \times f \geq 0$, which

means that y must lie on the left side of the force line. When $\omega \geq 0$ the object \mathcal{B} executes a counterclockwise rotation about y . In this case the inequality becomes $(x - y) \times f \leq 0$, implying that y must lie on the right side of the force line.

In our case $\mathcal{W}'_i = (\mathcal{W}_i^L)' \cap (\mathcal{W}_i^R)'$. When the intersection is performed on \mathcal{B} 's instantaneous rotations associated with $(\mathcal{W}_i^L)'$ and $(\mathcal{W}_i^R)'$, we obtain two labeled polygons. A polygon of counterclockwise rotations, denoted M_i^- , and a polygon of clockwise rotations, denoted M_i^+ (note that M_i^- corresponds to *positive* rotations while M_i^+ corresponds to *negative* rotations). The pair (M_i^-, M_i^+) represents the polar cone \mathcal{W}'_i . As depicted in Figure 4.13(b), this pair complements the friction cone C_i and its negative reflection with respect to x_i . Consider now the intersection of the k negative polygons, $M^- = \cap_{i=1}^k M_i^-$, and the intersection of the k positive polygons, $M^+ = \cap_{i=1}^k M_i^+$. If M^- or M^+ becomes empty during the intersection process, it is marked as an empty set. The pair (M^-, M^+) graphically represents the polar cone $\mathcal{W}'_1 \cap \dots \cap \mathcal{W}'_k$. Note that M^- and M^+ are constructed as intersection of convex sets. Since the intersection of convex sets is convex, M^- and M^+ are convex and therefore connected sets.

Our final step is to depict the cone $\mathcal{W}_1 + \dots + \mathcal{W}_k$ by identifying the meaning of polarity with respect to the instantaneous rotations associated with the pair (M^-, M^+) . According to Poinso't's theorem (Theorem ??), the wrenches acting on a planar object \mathcal{B} can be parametrized as force lines, $(f, \tau) = (f, x \times f)$, where f is a force acting on \mathcal{B} along a line passing through x . The following lemma describes the collection of force lines polar to the instantaneous rotations of the pair (M^-, M^+) .

Lemma 4.5.2 (Moment Labeling). *Let M^- and M^+ be the counterclockwise and clockwise instantaneous rotation polygons, representing the polar cone $\mathcal{W}'_1 \cap \dots \cap \mathcal{W}'_k$. The net wrench cone, $\mathcal{W} = \mathcal{W}_1 + \dots + \mathcal{W}_k$, consists of all force lines $(f, x \times f)$ satisfying the condition:*

$$\mathcal{W} = \left\{ \begin{pmatrix} f \\ x \times f \end{pmatrix} : (x-y) \times f \leq 0 \text{ for all } y \in M^- \text{ AND } (x-y) \times f \geq 0 \text{ for all } y \in M^+ \right\}.$$

The force lines of \mathcal{W} thus generate **negative semi-definite** torque about all points of M^- , and **positive semi-definite** torque about all points of M^+ .

Proof: Let us embed the planar environment as the (x, y) plane in \mathbb{R}^3 , and let $\mathbf{e} = (0, 0, 1)$ be a unit vector perpendicular to the (x, y) plane. Under this embedding \mathcal{B} 's angular velocity is given by $\omega \mathbf{e}$ for $\omega \in \mathbb{R}$. According to Chasles' Theorem (Theorem ??), the tangent vectors $\dot{q} = (v, \omega) \in T_{q_0} \mathbb{R}^3$ can be represented as instantaneous rotations of magnitude ω about points y in the plane. The parametrization of $\dot{q} = (v, \omega)$ in terms of y and ω is as follows. Let b be a fixed point on \mathcal{B} , described in \mathcal{B} 's frame. The world position of b at $q_0 = (0, \theta_0)$ is given by $y = R(\theta_0)b$. When \mathcal{B} moves with c-space velocity \dot{q} , the velocity of y is given by $\dot{y} = \omega \mathbf{e} \times y + v$. The center of rotation associated with \dot{q} is the point y whose velocity vanishes, $\dot{y} = \omega \mathbf{e} \times y + v = \vec{0}$. Hence $v = -\omega \mathbf{e} \times y$, and the desired parametrization is $\dot{q} = \omega(y \times \mathbf{e}, \mathbf{e})$ for $(y, \omega) \in \mathbb{R}^2 \times \mathbb{R}$. Substituting for \dot{q} in the polarity condition (4.7) gives

$$\begin{pmatrix} f \\ x \times f \end{pmatrix} \cdot \dot{q} = \omega(f, x \times f) \begin{pmatrix} y \times \mathbf{e} \\ \mathbf{e} \end{pmatrix} = \omega((x - y) \times f) \cdot \mathbf{e} \leq 0.$$

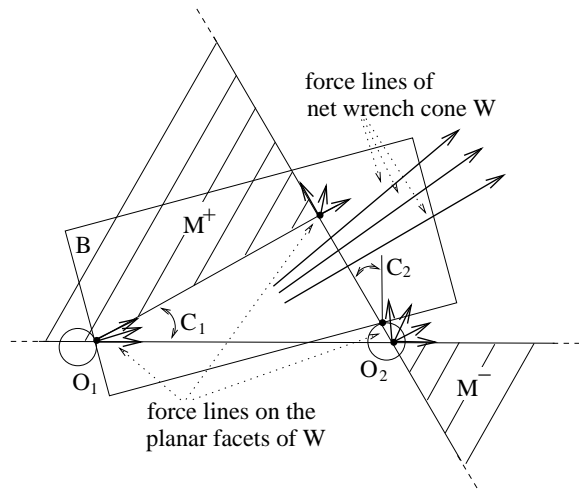


Figure 4.14: The instantaneous rotation polygons M^- and M^+ and the force lines spanning the net wrench cone $\mathcal{W} = \mathcal{W}_1 + \mathcal{W}_2$.

There are now two cases to consider. When $y \in M^-$, \mathcal{B} executes a counterclockwise rotation about y . In this case $\omega \geq 0$, and the polarity condition becomes $((x - y) \times f) \cdot e \leq 0$. When $y \in M^+$, \mathcal{B} executes a clockwise rotation about y . In this case $\omega \leq 0$, and the polarity condition becomes $((x - y) \times f) \cdot e \geq 0$. These two requirements give the force lines of the net wrench cone. \square

Example: Figure 4.14 shows a frictional two-finger grasp of a rectangular object. Assuming frictional point contacts, the figure depicts the M^- and M^+ polygons for this grasp. The net wrench cone generated by the two contacts, $\mathcal{W}_1 + \mathcal{W}_2$, corresponds to all force lines passing between M^- and M^+ such that the lines generate negative semi-definite moments about *all* points of M^- , and positive semi-definite moments about *all* points of M^+ . Since $\mathcal{W}_1 + \mathcal{W}_2$ is the sum of two planar sectors based at the wrench space origin, it is a tetrahedral cone analogous to the one depicted in Figure 4.12(b). The planar facets of $\mathcal{W}_1 + \mathcal{W}_2$ correspond to force lines passing through the vertices of M^- and M^+ (see exercise 4.x). In this example M^- and M^+ have a total of three vertices, and $\mathcal{W}_1 + \mathcal{W}_2$ is therefore bounded by three planar facets in wrench space.

Exercise: Consider a planar two-finger grasp, such as the one depicted in Figure 4.14. Assuming frictional point contacts, the net wrench cone, $\mathcal{W}_1 + \mathcal{W}_2$, forms a cone based at the wrench space origin and bounded by planar facets. Prove that the planar facets of this cone correspond to force lines passing through the vertices of the instantaneous rotation polygons M^- and M^+ .

Solution: The planar facets of $\mathcal{W}_1 + \mathcal{W}_2$ correspond to flat pencils of force lines (see Chapter ??). Consider now a flat pencil based at x_0 . When x_0 is located at a vertex of M^- or M^+ , some perturbations of x_0 move it into the interior of either M^- or M^+ , while other perturbations move it into the exterior of both polygons. It follows that such a pencil corresponds to a boundary facet of $\mathcal{W}_1 + \mathcal{W}_2$. Note that when x_0 is located at an interior point of an edge of M^- or M^+ , only a single force line of the pencil is feasible. This force line corresponds to a wrench aligned with an edge of the net wrench cone.

Exercise: Consider the two-finger grasp depicted in Figure 4.14. The net wrench cone, $\mathcal{W}_1 + \mathcal{W}_2$, is a tetrahedral cone bounded by three planar facets. Determine which positions of \mathcal{O}_2 along the edge of \mathcal{B} transform the net wrench cone into a four-sided tetrahedral cone.

Solution: When the contact point of \mathcal{O}_2 with \mathcal{B} slides leftward outside the friction cone C_1 , the polygons M^- and M^+ possess four vertices. Since the vertices of M^- and M^+ correspond to the planar facets of $\mathcal{W}_1 + \mathcal{W}_2$ in wrench space, in this case $\mathcal{W}_1 + \mathcal{W}_2$ is bounded by four planar facets.

Identifying Equilibrium Grasps. Let us now see how the moment labeling technique can identify equilibrium grasps. If a contact arrangement is a feasible equilibrium grasp, its net wrench cone contains at least an entire one-dimensional subspace passing through the wrench space origin (exercise 3.x). Equivalently, the contact arrangement can generate anti-parallel forces lying on a common line l . Now choose a positive direction for l . Since the contacts can generate a force line along l 's positive direction, M^- must lie on the left side of l while M^+ must lie on the right side of l . Since the contacts can also generate a force line along l 's negative direction, M^- and M^+ must also lie on the opposite sides of l . It follows that at an equilibrium grasp M^- and M^+ can be at most *subsets of a common line* l . Since M^- and M^+ are convex and therefore connected sets, each of these sets is either empty, a single point, or a single segment along the common line l . In particular, when $M^- = M^+ = \emptyset$ all force lines are feasible. This is the important case of *force closure*, where the net wrench cone fills the entire wrench space (see Chapter Z).

Exercise: Consider the three-finger grasp of a triangular object depicted in Figure 4.15(a). The grasp involves three *frictionless* contacts, such that the contact normal pass through a common point x_0 . Construct the M^- and M^+ polygons for this grasp. Determine if it is a feasible equilibrium grasp. Describe the force-lines corresponding to the net wrench cone.

Solution: For frictionless contacts, the regions M_i^- and M_i^+ are complementary halfplanes separated by the i^{th} contact normal line. The intersection of these regions gives $M^- = M^+ = \{x_0\}$. This is indeed an equilibrium grasp. Since x_0 belongs to both polygons, the force lines of the net wrench cone must generate zero moment about x_0 . Based on the moment formula, $\tau = x_0 \times f$, the feasible force lines can have any direction but must pass through x_0 . The resulting collection of force lines is a flat pencil of lines based at x_0 . The net wrench cone is therefore a two-dimensional subspace passing through the wrench space origin.

Exercise: Consider a slight shift of the finger \mathcal{O}_1 as shown in Figure 4.15(b). Repeat the previous exercise for the perturbed grasp arrangement.

Solution: Now $M^- = \emptyset$, while M^+ is a polygon with a non-empty interior. This contact arrangement is not a feasible equilibrium grasp, since no matter how we modulate the force magnitudes, all forces generate a strictly positive moment about all points of M^+ .

Exercise: Consider the four-finger grasp involving an additional finger, \mathcal{O}_4 , as depicted in Figure 4.15(c). Repeat the previous exercise for the four-contact arrangement.

Solution: When \mathcal{O}_4 is added M^+ becomes empty and in this grasp $M^- = M^+ = \emptyset$. This four-contact arrangement is therefore a feasible equilibrium grasp. Since all force lines are feasible, the net wrench cone covers the entire wrench space. This is an example of a force closure grasp (see Chapter Z).

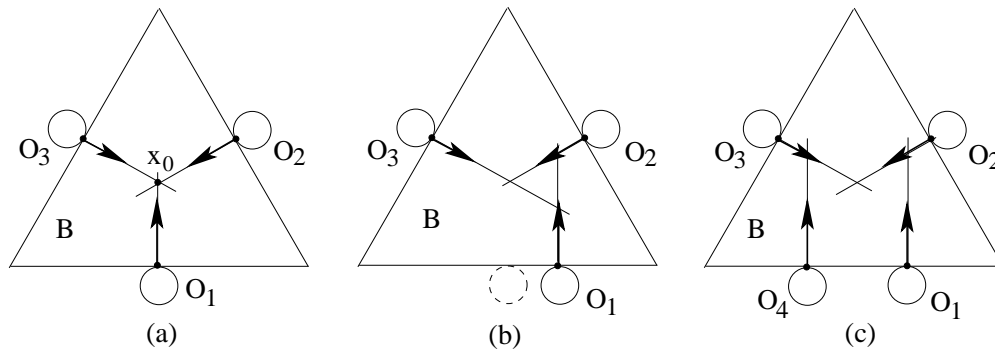


Figure 4.15: (a) A frictionless 3-contact grasp with concurrent force lines. (b) A slightly perturbed frictionless 3-contact grasp. (c) A frictionless 4-contact grasp.

Exercises

Exercise 4.1: A *line contact* occurs when a finger body touches the object \mathcal{B} along a line segment. The contact of a knife edge on flat surface is an example of such a contact. Assume that the Coulomb friction model holds at each point of the line contact. Show that a line segment contact can be replaced (or is equivalent to) a contact consisting of two distinct contact points placed along the line segment.

Solution:

Exercise 4.2: Let k point masses move freely in a planar environment. We wish to interconnect the points by rigid bars via rotational joints, such that the resulting structure would become a single rigid body. Assume that every pair of adjacent bars is connected by a single-degree-of-freedom rotational joint. Verify that $2k-3$ rigid bars suffice to interconnect k point masses into a single rigid structure.

Solution: When $k = 2$, a single bar connects two point masses into a rigid body. Hence consider the case of $k \geq 3$ point masses in \mathbb{R}^2 . Arrange the k points in a circle and interconnect these points by a circle of k bars. In general, three rigid bars connected by three rotational joints form a rigid triangle (this can be checked with Grübler's formula). Hence we can select one point mass on the circle, and connect it with every other point mass which is not adjacent to it along the circle. The resulting triangulated structure forms a single rigid body, and the structure has a total of $k + (k - 3) = 2k - 3$ bars.

Exercise 4.3: Under the conditions of the previous exercise, prove that $2k-3$ is the *minimum* number of rigid bars required to connect k points masses into a single rigid structure.

Solution: A structure made of rigid bars connected by rotational joints has two types of degrees of freedom. *Internal* degrees of freedom associated with rotation of the structure's joints, and *external* degrees of freedom associated with translation and rotation of the structure as a whole. The total number of internal degrees of freedom can be computed using Grübler's formula as follows. Consider a planar structure consisting of n bars attached by rotational joints. The initially disconnected bars have $3n$ degrees of freedom. Each attachment of two bars with a rotational joint reduces the total number of degrees of freedom by two. Since a planar structure has three external degrees of freedom, the total number of

internal degrees of freedom is $3(n - 1) - 2j$, where j is the number of pairwise attachments of bars in the structure.

Let us next derive a relation between the number of joints, j , and the number of point masses, k . The structure forms a graph whose nodes are the k point masses. Let d_i be the number of bars emanating from the i^{th} node. The number of joints at the i^{th} node is $d_i - 1$. Hence the total number of joints is given by $j = \sum_{i=1}^k (d_i - 1) = \sum_{i=1}^k d_i - k$. Each bar is attached at its two endpoints to the structure's nodes. Hence the sum of the node degrees satisfies the relation $\sum_{i=1}^k d_i = 2n$. Substituting $j = 2n - k$ in Grübler's formula gives: $3(n - 1) - 2j = 3(n - 1) - 2(2n - k) = 2k - n - 3$. The structure forms a rigid body when $2k - n - 3 \leq 0$. Any connection of k points masses into a rigid structure thus requires $n \geq 2k - 3$ bars.

Exercise 4.4: The two-finger grasp of the rectangular box depicted in Figure 4.7 is an example of a force closure grasp. Theoretically, the fingers can generate any desired net wrench on \mathcal{B} . List practical limitations to this statement.

Solution: From the object's perspective, its overall structural strength may limit the magnitude of the allowed finger forces. From the fingers' perspective, they are driven by mechanisms whose actuators are upper bounded by practical considerations such as motor strength and power supply limitations.

Exercise 4.5: Prove that each wrench cone $\mathcal{W}_i = \{(f_i, x_i \times f_i) : f_i \in C_i\}$ forms a cone in wrench space. Prove that the sum $\mathcal{W}_1 + \dots + \mathcal{W}_k$ is still a cone in wrench space.

Exercise 4.6: We described a procedure for connecting k spatial point masses into a rigid structure of $3k - 6$ rigid bars connected by spherical joints. Verify that the structure forms a single rigid body up to self-rotation of the bars.

Solution: Since the rigid bars are connected by spherical joints, the structure has two types of *internal* degrees of freedom: self rotations of the bars about their axes, and rotations of the structure's joints while the bars are fixed with respect to their axes. The structure also has six *external* degrees of freedom associated with translation and rotation of the structure as a whole. A spatial n -bar structure forms a rigid body when it has n internal degrees of freedom, as these degrees of freedom correspond to self-rotations of the n bars. The initially disconnected bars have $6n$ degrees of freedom. Each attachment of two bars with a spherical joint reduces the total number of degrees of freedom by three. Based on Grübler's formula, the structure's total number of *internal* degrees of freedom is $6(n - 1) - 3j$, where j is the number of pairwise attachments of bars, or joints, in the structure. The procedure uses a total of $n = 3k - 6$ bars to connect the k point masses. Each of the planar graphs is constructed with $\frac{k}{2} + 2(\frac{k}{2} - 3) = \frac{3}{2}k - 6$ joints. The k vertical bars are attached with $2k$ additional joints. The total number of joints is thus $j = 2(\frac{3}{2}k - 6) + 2k = 5k - 12$. Substituting for j in Grübler's formula, then using the relation $3k = n + 6$, gives: $6(n - 1) - 3j = 6(n - 1) - 3(5k - 12) = 6(n - 1) - 5(n + 6) + 36 = n$. Since the structure consists of n bars that can freely rotate about their axes, it forms a rigid body up to self-rotations of its bars.

Exercise 4.7: We have shown that k spatial point masses can be connected with $3k - 6$ rigid bars via spherical joints into a rigid structure. Prove that $3k - 6$ is the *minimum* number of bars required for this task.

Solution: A spatial structure of rigid bars connected by spherical joints has three types of degrees of freedom. The first type are *self rotations* of the bars about their axes. The second type are *internal* degrees of freedom associated with rotation of the structure's joints while the bars are kept fixed with respect to their axes. The third type are *external* degrees of freedom associated with translation and rotation of the structure as a whole.

The total number of internal degrees of freedom can be computed using Grübler's formula as follows. Consider a spatial structure consisting of n bars attached by spherical joints. The initially disconnected bars have $6n$ degrees of freedom. Each attachment of two bars with a spherical joint reduces the total number of degrees of freedom by three. Since a spatial structure has six external degrees of freedom and n self-rotation degrees of freedom, the total number of *internal* degrees of freedom is $6(n-1) - n - 3j$, where j is the number of pairwise attachments of bars in the structure.

Let us next derive a relation between the number of joints, j , and the number of point masses, k . The structure forms a graph whose nodes are the k point masses. Let d_i be the number of bars emanating from the i^{th} node. The number of joints at the i^{th} node is $d_i - 1$. Hence the total number of joints is given by $j = \sum_{i=1}^k (d_i - 1) = \sum_{i=1}^k d_i - k$. Each bar is attached at its endpoints to two nodes of the graph. Hence the sum of the node degrees satisfies the relation $\sum_{i=1}^k d_i = 2n$. Substituting $j = 2n - k$ in Grübler's formula gives: $6(n-1) - n - 3j = 6(n-1) - n - 3(2n - k) = 3k - n - 6$. The structure forms a rigid body when $3k - n - 6 \leq 0$. Any connection of the k points masses into a rigid structure thus requires $n \geq 3k - 6$ bars.

Exercise: Let a 3D object \mathcal{B} be grasped by two frictional point contacts at an equilibrium grasp. Characterize the subspace of internal forces for this grasp.

Bibliography

- [1] M.T. Mason. Compliance and force control for computer controlled manipulators. *IEEE Trans. Syst. Man and Cybernetics*, SMC-11(6):418–432, 1981.